

# Fast Switching Dual Frequency Liquid Crystal Optical Retarder for Beam Steering Applications.

Andrii B. Golovin, Ye Yin, Sergij V. Shiyanovskii, and Oleg D. Lavrentovich  
Liquid Crystal Institute, Kent State University, Kent, Ohio, 44242-0001, USA  
Email: [odl@lci.kent.edu](mailto:odl@lci.kent.edu), Fax: (330)672-2796, Phone:(330)672-4844

*We demonstrate a fast optical modulator capable of switching large amount of optical retardation (a few microns) in less than 1 ms. The result is achieved by employing a dual frequency nematic in cells with high pre-tilt alignment and by providing a special addressing scheme that features amplitude and frequency modulated voltage. We explore the effect of time delay and dielectric heating in process of the optical retardation switching.*

*Keywords:* optical retarder, dual frequency nematic, response time, time delay, dielectric heating.

## 1. Introduction

Many electronic imaging devices require a scanning motion system with a “flying” light spot, derived typically from a laser source. Usually the scanning process is executed by rotating mirrors, acousto-optic deflectors, mirrors with piezoelectric actuators or by gradient (electro-optic) prisms [1]. One of the most promising non-mechanical approaches is the so-called Optical Phased Array (OPA) based on birefringent liquid crystal gratings formed in electrically driven flat cells with a system of striped electrodes [2, 3]. The maximum deflection angle of the OPA is determined by the thickness of the cell  $d$ , optical anisotropy of the LC material  $\Delta n = n_e - n_o$ , and an aperture D:

$$\delta_{\max} \approx \frac{\Delta L_{\max}}{D}, \quad (2)$$

where  $\Delta L_{\max} = \Delta n \cdot d$  is the maximum optical retardation shift achieved at one electrode,  $n_e$  and  $n_o$  are the extraordinary and ordinary indices of refraction respectively. A convenient way to increase the deflection angle is to enlarge the maximum optical retardation by increasing the thickness of LC cell. Unfortunately, a larger  $d$  leads to a slow response with the characteristic times [4]:

$$\tau_{on} = \gamma_1 d^2 / [\epsilon_0 |\Delta \epsilon| (U_{rms} - U_c)] \quad (3)$$

$$\tau_{off} = \gamma_1 d^2 / (\pi^2 K) \quad (4)$$

Here  $K$  is the effective elastic constant,  $\gamma_1$  is the characteristic rotational viscosity,  $\Delta \epsilon = \epsilon_{||} - \epsilon_{\perp}$  is the dielectric anisotropy,  $\epsilon_{||}$  and  $\epsilon_{\perp}$  are the dielectric permittivity components measured along and perpendicular to the director, respectively;  $\epsilon_0$  is the permittivity of free space,  $U_c$  is the threshold voltage of Frederiks transition in a cell with planar or homeotropic alignment, and  $U_{rms} > U_c$  is the actual applied voltage. The relevant Figure of Merit that depends on the switch-off time and characterizes the trade-off for the optical modulators,

$$FoM = \Delta L_{\max}^2 / \pi^2 \tau_{off}, \quad (5)$$

can be re-expressed exclusively in terms of the material parameters [5]:

$$FoM_m = K (n_e - n_o)^2 / \gamma_1. \quad (6)$$

The latest expression inspired many researchers to seek for the improvement of optical retarders by synthesizing new materials with a higher optical birefringence, lower viscosity and larger Frank constants. Recently, our group has demonstrated that *FoM* can be improved by two orders of magnitude by exploring a different method of switching rather than synthesizing new materials [6]. The idea is to use dual frequency nematic (DFN) in cells with high pre-tilt angle alignment and a special addressing scheme that features amplitude and frequency modulated voltage. In DFN,  $\Delta\epsilon > 0$  for  $f < f_c$  and  $\Delta\epsilon < 0$  for  $f > f_c$  where  $f_c$  is the so-called crossover frequency at which  $\Delta\epsilon = 0$ . The corresponding *FoM* (5) can be represented in terms of materials parameters and the applied voltage  $U$  [6]:

$$FoM \approx \frac{K \cdot \Delta n^2}{1.2\gamma_1} \left( 1 + \frac{U^2}{U_0^2} \right), \quad (7)$$

where  $U_0 = \sqrt{2K/(\Delta\epsilon \cdot \epsilon_0)}$ . Applying a high voltage to switch the state of the cell, one can increase *FoM* significantly, by orders of magnitude [6]. Note that the value of  $U$  determines also the value of phase retardation gained within the LC cell. For example, when  $\Delta\epsilon > 0$  and  $U \rightarrow \infty$  the director realigns perpendicularly to the bounding plates and  $\Delta L \rightarrow 0$ . Therefore, it is necessary to address the cell with a modulated voltage, namely, a high-amplitude pulse  $U = U_{SSP}$  of short duration (called Special Short Pulses, or SSP [6]), to speed up the process of director reorientation, followed by a holding- amplitude pulse  $U = U_{hold}$  (usually  $U_{hold} \ll U_{SSP}$ ) that maintains the desired level of phase retardation.

The driving scheme with a frequency and amplitude modulated voltage described in [6] poses a number of interesting questions. First of all, the high amplitude pulses can heat the cell; temperature changes might shift the value of the critical frequency and thus change the value of  $\Delta\epsilon$ . Second, as the value of  $\Delta\epsilon$  is strongly dependent on the frequency of the applied voltage, it would be sensitive to the shape of the pulses and to their duration.

In this paper, we address these issues of fast switching DFN. We develop the model and test dielectric heating of the cells and explore the delay between the front of the voltage pulses and optical (director-mediated) response of the cell.

## 2. Fast modulation of optical retardation

According to Eqs.(3), (4), one can decrease  $\tau_{on}$  by increasing the applied voltage. However, in usual nematics the switch-off time  $\tau_{off}$  depends only on the material parameters and is proportional to  $d^2$ , so that it cannot be shortened by a higher electric field. In contrast, a DFN cell can be driven by a high-amplitude voltage in both directions, depending on the frequency of the applied voltage, because the dielectric anisotropy  $\Delta\epsilon$  changes the sign at crossover frequency. For example, the nematic material MLC-2048 has  $\Delta\epsilon = 3.22$  at frequency 1 kHz and  $\Delta\epsilon = -3.08$  at 50 kHz at the room temperature, as it shown in Fig.1. Using that feature one can control the switching dynamics of DFN cell in **both** directions by the applied voltage.

In our experiments we used the nematic cells which were assembled in an anti-parallel fashion from glass plates coated with a conducting Indium Tin Oxide (ITO) and obliquely deposited thin SiO layers ( $\approx 20$  nm). The latter yield a high pre-tilt angle  $\alpha_b$  the director **n** makes with the substrate. In what follows, we describe cells with  $\alpha_b \approx 45^\circ$ , although the results were similar for a much broader range of angles  $10^\circ \leq \alpha_b \leq 80^\circ$ . Electric voltage aligns **n** perpendicularly to the plates (the so-called homeotropic state) when  $f < f_c$ , and parallel to the plates when  $f > f_c$ . Here a high value of pre-tilt angle has several advantages. First, the dielectric torque of the applied field is maximized when the angle between the director and the field is about 45 degrees; second, there is no threshold for director reorientation; third, the high pre-tilt guarantees strong restoring surface torques that facilitates reorientation from both the homeotropic and the planar states.

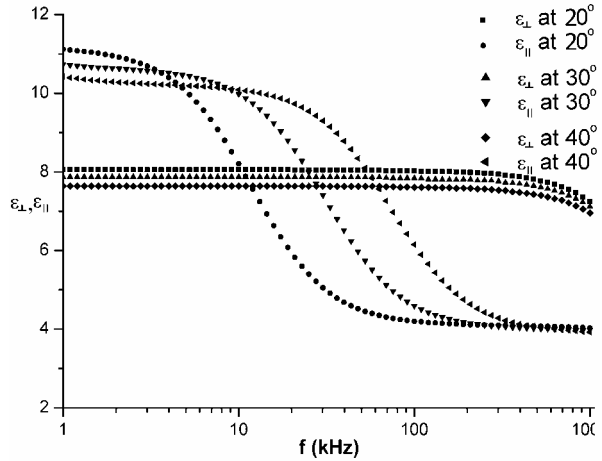


Fig. 1. Frequency (logarithmic scale) dependent dielectric permittivities  $\epsilon_{\parallel}$  and  $\epsilon_{\perp}$  at  $20^{\circ}\text{C}$ ,  $30^{\circ}\text{C}$ , and  $40^{\circ}\text{C}$ .

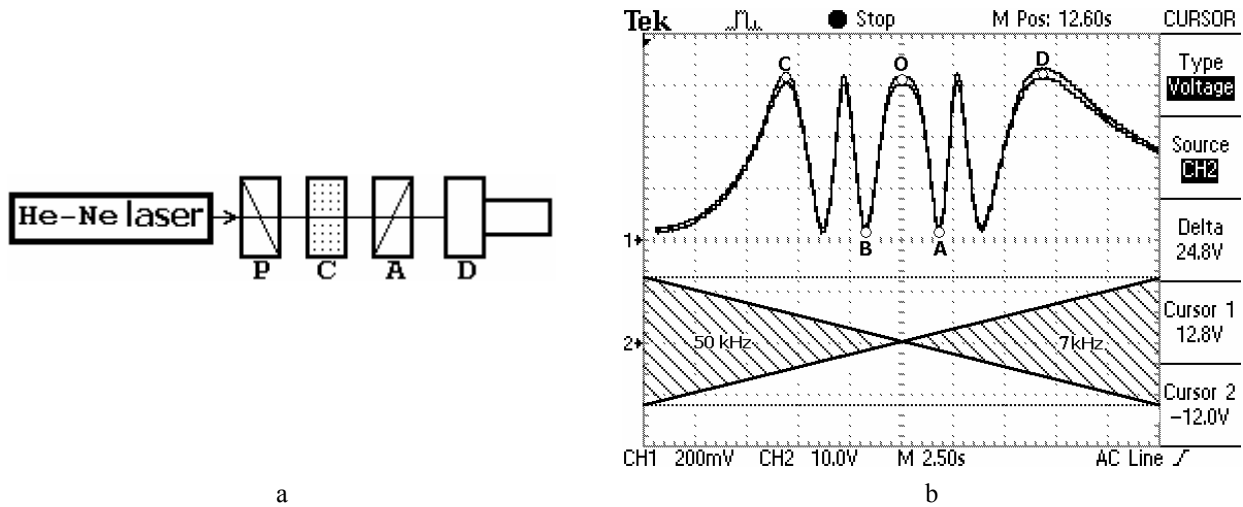


Fig.2. Optical setup: a) He-Ne laser ( $\lambda \approx 633\text{nm}$ ), P is polarizer, C is LC cell, A is analyzer, D is photodiode; b) photodiode signal (top) vs. amplitude and frequency of the applied voltage (bottom).

We carried out the experiments at elevated temperature  $32^{\circ}\text{C}$ , where  $f_c = 31\text{ kHz}$ . This allowed us to decrease the rotational viscosity and also to use a relatively high frequency of  $7\text{ kHz}$  to drive the cell in the “low-frequency” regime. The high-frequency driving voltage was applied at  $50\text{ kHz}$ . The voltage dependence of phase retardation was measured in a standard fashion, with the DFN cell of thickness  $d=14.5\text{ }\mu\text{m}$  placed between two crossed polarizer prisms, Fig.2.

In the optical setup we tested the switching time of DFN cell. In that case, the projection of director  $\mathbf{n}$  onto the cell substrates makes an angle  $45^{\circ}$  with the axes of polarizer and the analyzer, so the intensity of transmitted light follows the rule:  $I = I_0 \sin^2 \left[ \frac{\pi \cdot \Delta L(U)}{\lambda} \right]$ , where  $I_0$  is the intensity of incident light (we neglect small corrections caused by

reflection at interfaces, scattering at director fluctuations, etc.) and  $\lambda$  is the wavelength of light [7] and  $\Delta L(U)$  is the voltage-dependent retardation acquired in the birefringent LC cell. Figure 2 shows  $I$  (top trace) vs. applied voltage  $U_{rms}$  at frequencies  $7$  and  $50\text{ kHz}$  (bottom trace). The variation of  $I$  between the two neighboring minima (e.g., A and B in Fig.2) corresponds to the retardation shift  $\Delta L_{AB} = 633\text{ nm}$ .

We optimized the driving scheme for DFN cell by including SSPs of high-amplitude (at both driving frequencies) to initiate fast director reorientation, followed by a relatively low voltage to keep the retardation at the desired level. The oscilloscope pictures of fast switching at relatively small ( $\Delta L_{OA} \approx 0.3 \mu m$ ) and large ( $\Delta L_{CD} = 2.5 \mu m$ ) optical retardations are demonstrated in Fig.2 and 3, respectively. In Fig.2, the first SSP (duration  $100 \mu s$ ,  $U_{rms} = 50 V$ ) triggers a fast reorientation towards the homeotropic state. A square-wave holding voltage  $U_{rms} = 2 V$  at  $7 kHz$  follows to hold the cell in the state A (the states are labeled as in Fig.1). The A state is switched back into the initial O state by a second SSP (duration  $120 \mu s$ ,  $U_{rms} = 25 V$  at  $50 kHz$ ); the holding voltage is zero for the state O.

Figure 3 shows C↔D transition, switched with SSPs of  $100 V$  amplitude. The switching times are  $\sim 0.5 ms$ . Some features of fast switching are worth mentioning. First, there is a small time delay ( $30-50 \mu s$ ) between the initial front of an SSP and the corresponding front of the photodiode signal (Figs.2, 3), we explore this feature in the section 3. Second, the transient maxima and minima seen in Fig.3 are relatively small (meaning that the modulation of light intensity is not complete). There are few possible reasons of this effect: (a) in-plane non-homogeneity of pre-tilt angle, anchoring energy, surface viscosity, etc.; (b) the structural transition can be accompanied by an in-plane flow, which in turn may cause director dynamics.

Let us briefly discuss the advantages of the high pre-tilt cells over the regular planar or homeotropic cells. As seen from Eq.(3) and (7), the response time depends on the elastic constant  $K$ , and one can expect that the homeotropic cell might have a faster response than a cell with either planar or high pre-tilt alignment, as the corresponding splay constant is generally smaller than that of bend. The homeotropic cell is indeed capable of the fastest response, but there is a drawback as it is hard to achieve a uniform director reorientation. Even in the cells with rubbed homeotropic alignment layers, the director experiences in-plane distortions upon reorientation from the homeotropic to planar (or tilted) state. As the result, the cells with a high pre-tilt angle such as described in this work are the best overall choice.

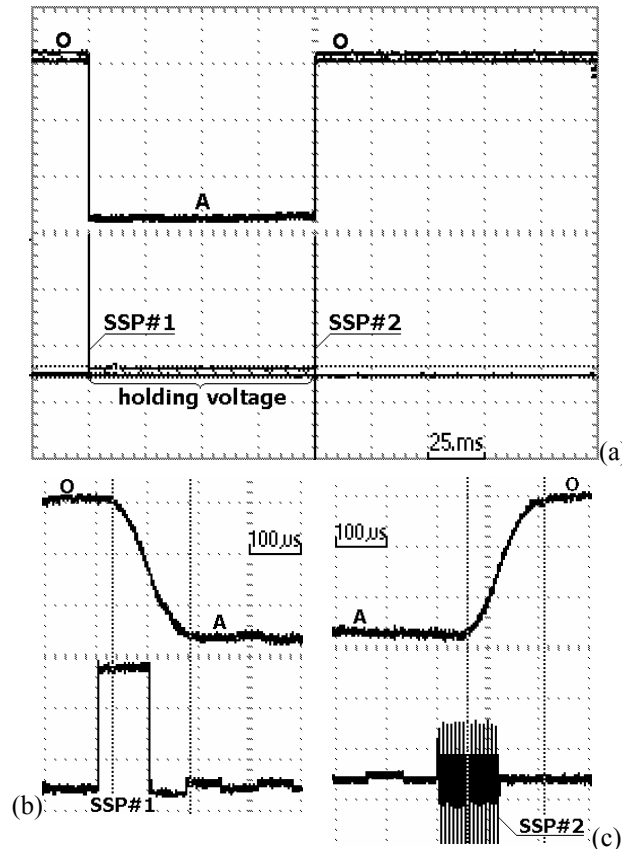


Fig.2. Fast phase shift on  $\Delta L = 0.3 \mu m$  by driven holding voltage  $7 kHz$  and two SSPs; a)  $25ms/sqr$ ; b,c)  $100 \mu s/sqr$ .

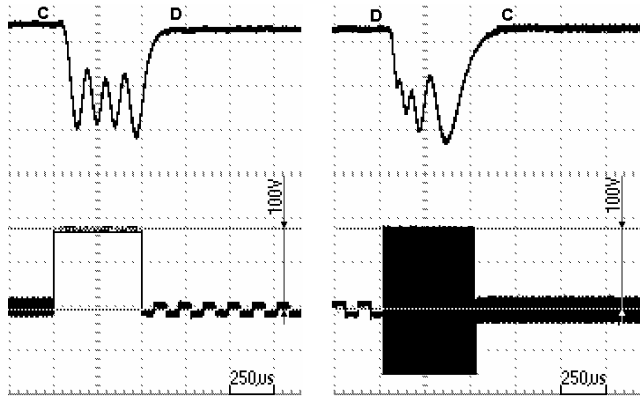


Fig.3. Fast switching on  $\Delta L = 2.5 \mu m$  during  $\tau \approx 0.5$  ms.

### 3. Time delay

In experiments with a fast switched dual frequency nematic cell, we observed a small time delay (about 30-60  $\mu s$ ) between the beginning of the SSP and optical response signal from photodiode (Figs.2 and 3).

To verify whether the time delay in dual-frequency material is related to the degeneracy of the phase retardation vs. voltage when the switching is performed between the extremal states with maxima and minima of the transmitted light intensity, we studied switching between the states in which the slope of the retardation-voltage curve is maximum. Figure 4a shows such a phase shift in DFN cell, when the amplitude of applied voltage was varied slowly. Figure 4b shows the fast shift by  $\Delta L \approx 0.3 \mu m$  under the applied voltage with the SSP and holding voltage at the frequency 7 kHz. The time delay is  $\Delta \tau \approx 25 \mu s$ . Therefore, the time delay is a general feature of DFN cells not related to particular regions in which the retardation vs. voltage curve has an extremum.

We compared the dynamics of relaxation of DFN MLC2048 to that one in two regular nematics E7 and 5CB. We found that the delay is noticeably smaller in regular nematics. For example, Figs.5 shows that the time delay is smaller than 10  $\mu s$  (the accuracy limit of our measurements) in switching of the nematic cell with gap thickness 10  $\mu m$  filled with 5CB.

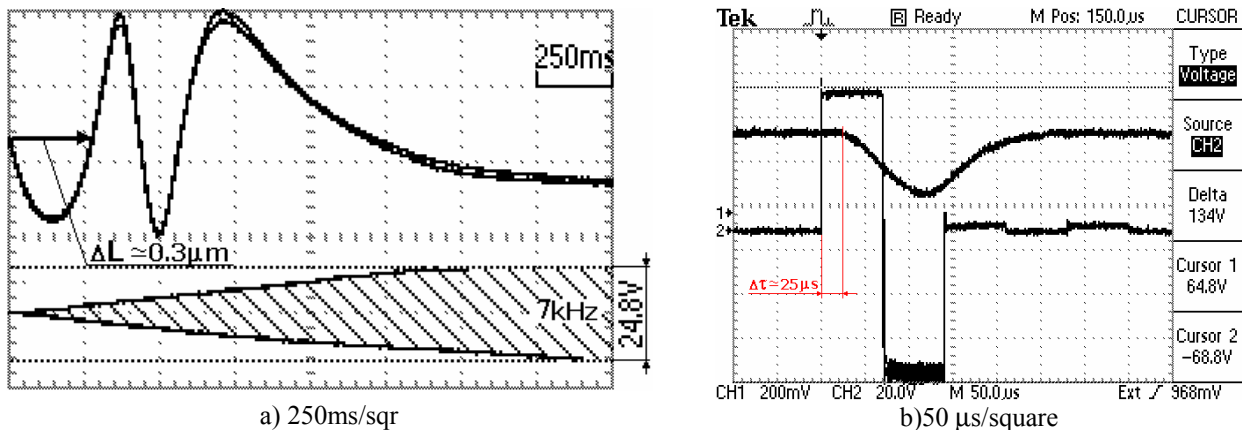


Fig.4. Optical retardation switching on  $\Delta L \approx 0.3 \mu m$  (b) between two non-extremal points in transmitted signal of the optical setup.

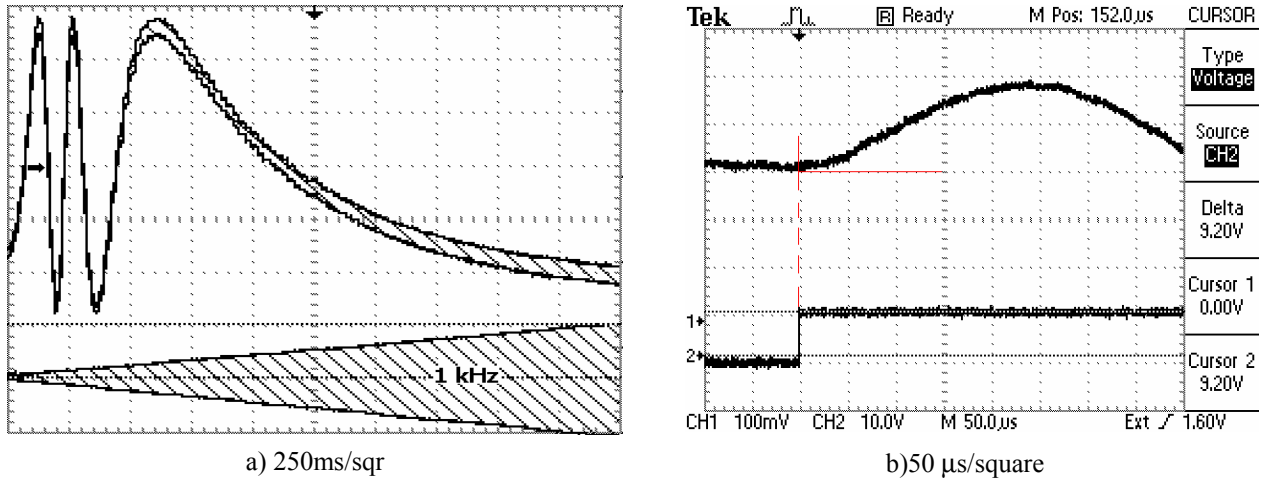


Fig.5. Phase shift by 10  $\mu\text{m}$  thick 5CB cell with high pretilt angle ( $\alpha \approx 37^\circ$ ).

We also checked the Fourier spectrum of the initial wavefront of high and low frequency SSP's, because the dielectric anisotropy of DFN material is frequency-dependent. The sharp front of the applied voltage pulse corresponds to a broad frequency range of the Fourier spectrum with a decrease of the effective dielectric anisotropy; this might cause the delay in the cell's response. We checked the Fourier spectrum of SSP's wave-front, by using the built-in Fast Fourier Transformation (FFT) function of Tektronix oscilloscope TDS2014 in the amplification mode of spectral components with frequencies lower than 20 MHz. For example, oscilloscope pictures in Fig.6a and 7a show the initial wavefronts of low and high frequencies SSP with amplitude  $U_{rms}=50V$ , oscilloscope pictures in Fig.6b and 7b show the corresponding spectra of FFT. The spectra of the initial wavefronts of high frequency SSP with amplitude  $U_{rms}=50V$  (Fig.8b, 9b, 10b) are shown in Fig.8d, 9d, 10d.

Two possible scenarios of time delay could appear depending on the spectral distribution of the FFT spectrum of the initial wavefront of SSP according to Figs. 6, 7. One scenario has a broad first FFT harmonic ( $>50 \text{ kHz}$ ), where the maximum of the spectral density is close to crossover frequency  $f_c$ , as shown in Fig.6. In that case, the square waveform of high frequency applied voltage does not change the phase retardation of transmitted light during the first  $\sim 50 \mu\text{s}$  because within this time range  $\Delta\epsilon$  is effectively zero. After that time the spectrum of high frequency applied voltage becomes narrower with the maximum amplitude of spectral density at 50 kHz and thus the director of DFN cell reorients perpendicularly to the applied electric field.

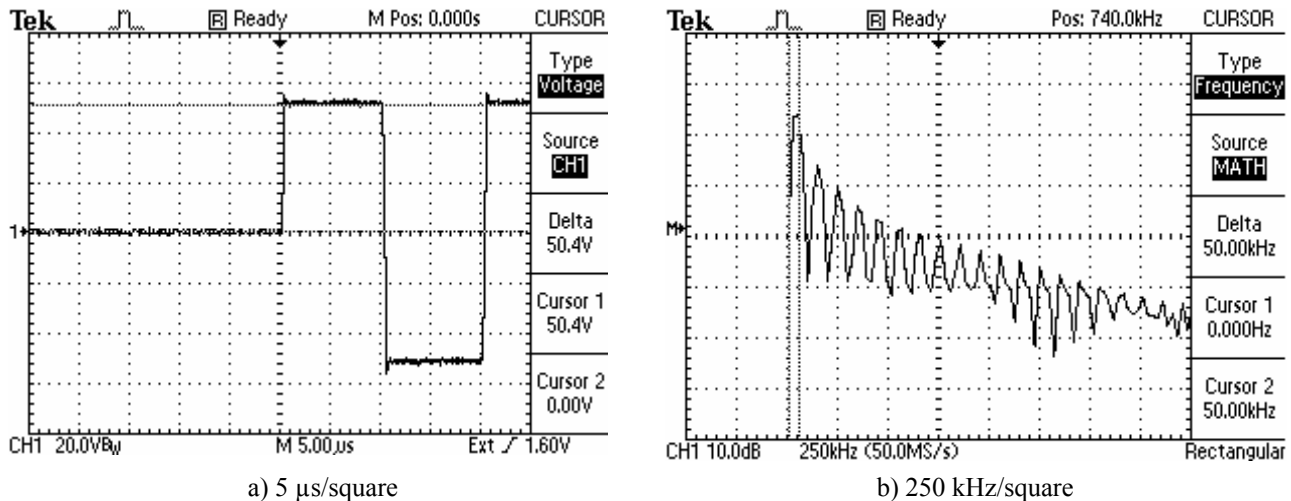


Fig.6. Initial wavefront of the Special Short Pulse at high frequency (a); and corresponding Fast Fourier Transform spectrum (b), where two vertical markers show the spectral interval of width 50 kHz.

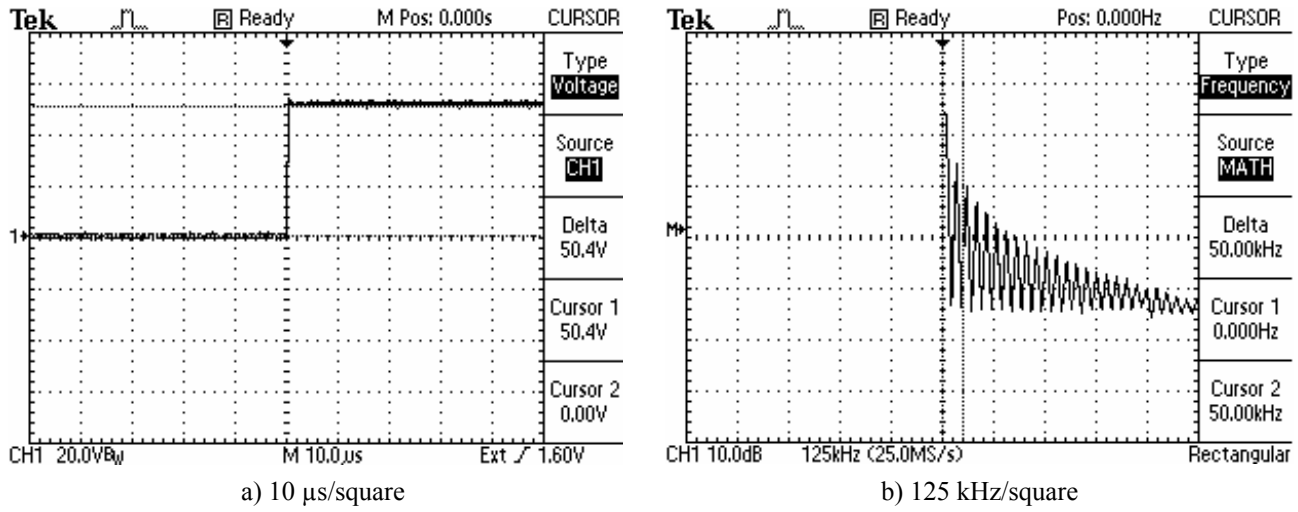


Fig.7. Initial wavefront of the Special Short Pulse at low frequency(a); and corresponding Fast Fourier Transform spectrum (b), where two vertical markers show the spectral interval of width 50 kHz.

Another scenario is shown in Fig.7, where the square waveform applied voltage at low frequency has approximately equal amplitudes of FFT harmonics at  $f < f_c$  and at  $f > f_c$ . In that case the square waveform pulse of low frequency applied voltage activates positive and negative signs of the dielectric anisotropy simultaneously during first 30  $\mu s$ . During this time the resulting phase retardation of the transmitted light is close to zero. After this time the spectrum of low frequency applied voltage changes the distribution of spectral amplitudes and it becomes narrower with maximum at 1 kHz. Thus the director of DFN cell reorients parallel to applied electric field.

Features of DFN material mentioned above help to reduce further the switching time in the dual-frequency nematic cell. For example, the profile of the SSP could be modified with a special waveform, as shown in Fig.8. The initial front of the SSP contains short pulses with decreasing amplitudes and the main part of the pulse is a half-period sinusoidal wave. Short pulses influence both parts of dielectric anisotropy and increase the time delay up to 50  $\mu s$ . The main pulse affects the positive part of dielectric anisotropy only. The level of transmitted signal starts to change in the moment of minimum amplitude of high frequency pulses of applied voltage and maximum amplitude of low-frequency applied voltage. The high amplitude of the half-period sinusoidal SSP stimulates the fast phase shift. The holding voltage completes the process of reorientation. The total time of optical retardation switching at  $\Delta L \approx 0.3 \mu m$  is about  $\tau \approx 100 \mu s$ .

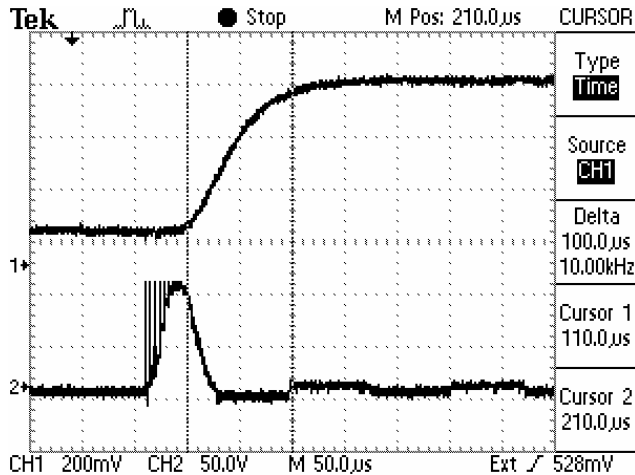


Fig.8. Switching of the optical retardation  $\Delta L \approx 0.3 \mu m$  during  $\tau \approx 100 \mu s$  by the applied voltage with special form SSP (50  $\mu s$ /square).

#### 4. Dielectric Heating

The presented results (e.g. Fig.1) show that material parameters that control the optical switching of a DFN cell strongly depend on the cell temperature. Electric field induced heating thus might affect the performance of DFN cells. The temperature raise of the LC film is controlled by the heat transfer from the cell and can be presented as a sum of two terms. The first term is the temperature difference between the LC and the external surfaces of cell substrates. It is determined by the thickness and thermal conductivity of the substrates. The second term is the temperature raise at the external surfaces of cell substrates. It depends mostly on air convection outside the cell and can vary significantly for different experimental conditions. Our goal is to study the temperature gradient inside the cell because the contributions of two terms are independent for permanent heating and the temperature at the external surfaces of cell substrates can be easily measured during the experiment.

To detect the temperature gradient inside a cell we used the LC film of the thickness  $d = 25 \mu m$  covered with glass substrates of the thickness  $l = 1.1 mm$ . The E-type thermocouple CHCO-0005 (Omega Inc.); which has high accuracy ( $\sim 0.05^\circ C$ ), fast response ( $< 10 ms$ ) and small size ( $\sim 25 \mu m$ ), was placed inside the cell. The dielectric layer (AT720) is spin-coated on the ITO (indium tin oxide) electrodes at the glass surfaces to insulate them from the thermocouple. The cell was initially thermally stabilized in a Linkam hot stage and then heating voltage was applied.

The glass substrates are usually much thicker than the LC film, thus the heat losses in the LC film are negligibly small and its temperature is controlled by the temperature gradient in the substrates. The kinetics of the temperature field  $T(x, t)$  in the glass substrates with density  $\rho$ , heat capacity  $c_p$  and heat conductivity  $G$  is determined by the heat conduction equation:

$$c_p \rho \frac{\partial T}{\partial t} = G \frac{\partial^2 T}{\partial x^2} \quad (8)$$

We assume that before heating ( $t = 0$ ) the whole substrate has the temperature  $T(x, 0) = T_0$  of the hot stage and that this temperature remains constant at the outer surface ( $x = 0$ ) of the substrate,  $T(0, t) = T_0$ . The boundary condition at the inner surface of the glass substrate ( $x = l$ ) is determined by the heat transfer from the LC film

$$\left( \frac{\partial T}{\partial x} \right)_{x=L} = g = \frac{Pd}{2G} \quad (9)$$

where  $P$  is the power density absorbed by the cell:

$$P = 2\pi U_{rms}^2 f \epsilon''(f) / d \quad (9a)$$

and  $\epsilon''(f)$  is the imaginary part of the dielectric permittivity component along the applied field.

The solution of Eq. (8) reads:

$$T(t, x) = T_0 + gx - \sum_{n=0}^{\infty} \frac{(-1)^n 8gl}{\pi^2 (2n+1)^2} \exp\left[-\frac{(2n+1)^2 t}{\tau}\right] \sin\left[\frac{\pi(2n+1)x}{2l}\right] \quad (10)$$

where  $\tau = \frac{4l^2 c_p \rho}{\pi^2 G}$ . The 0<sup>th</sup> term in the sum is dominating, so the LC film temperature  $T_{LC}(t)$  may be approximated with:

$$T_{LC}(t) = T_0 + \Delta T [1 - \exp(-t/\tau)], \quad (11)$$

where  $\Delta T$  is the stationary LC film temperature raise:

$$\Delta T = gl = \pi U_{rms}^2 f \epsilon''(f) l / G , \quad (12)$$

The temperature response for applying the voltage of different amplitudes (Fig.9) and frequencies (Fig.10) of the cell placed in the thermally stabilized hot stages at temperature  $40^\circ C$  shows rather good agreement with presented model. All curves have approximately the same relaxation time  $\tau \approx 10s$ , however it is several times larger than expected. The discrepancy can be attributed to the thermocouple influence on the temperature response and to the insufficient thermal stabilization of the outer surface of the top substrate.

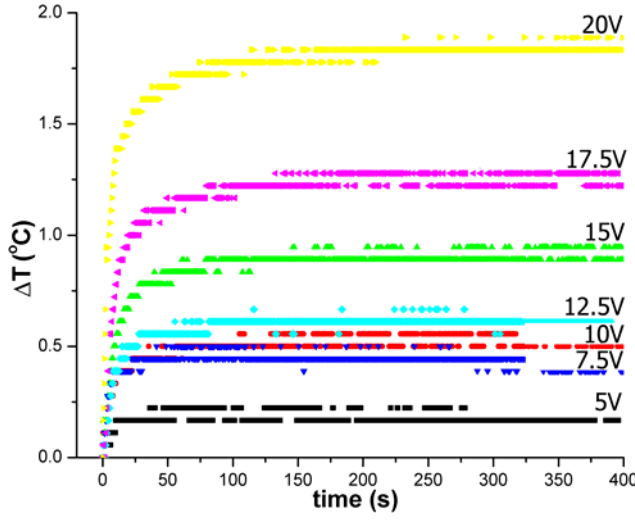


Fig.9. Temperature changes of DFN cell placed in the hot stages with stabilized temperature at  $40^\circ C$  after the different voltages  $U_{rms} = 5, 7.5, 10, 12.5, 15, 17.5$  and  $20$  V were applied at frequency  $1$  MHz.

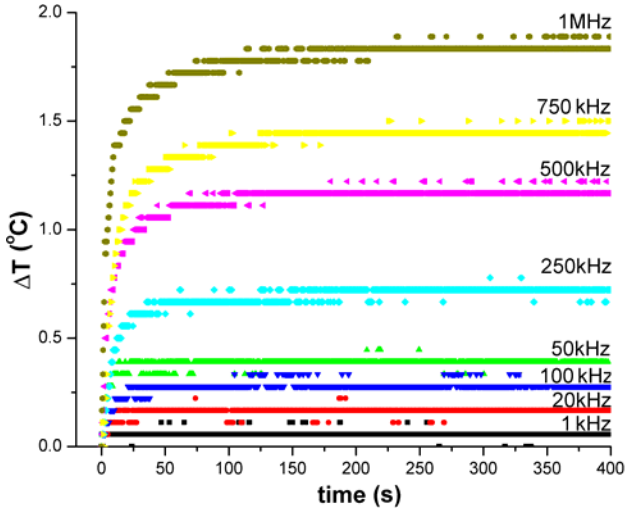


Fig.10. Temperature response of DFN cell placed in the hot stage with stabilized temperature at  $40^\circ C$  after the voltage  $U_{rms} = 20$  V were applied at frequencies:  $f = 1, 20, 50, 100, 250, 500, 750$  kHz and  $1$  MHz.

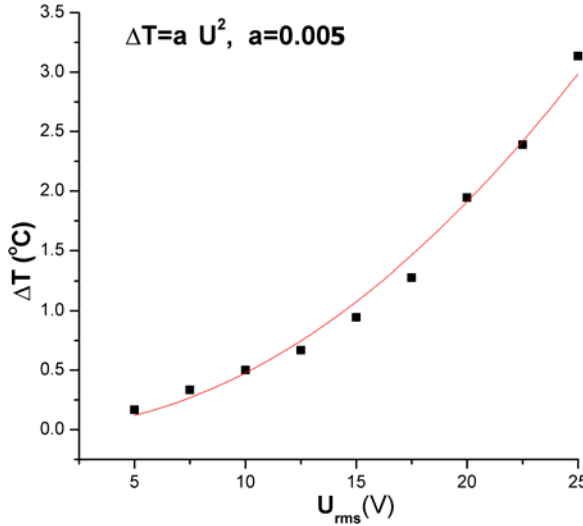


Fig.11. Stationary temperature change  $\Delta T$  is proportional to  $U_{rms}^2$ ,  $f=1$  MHz.

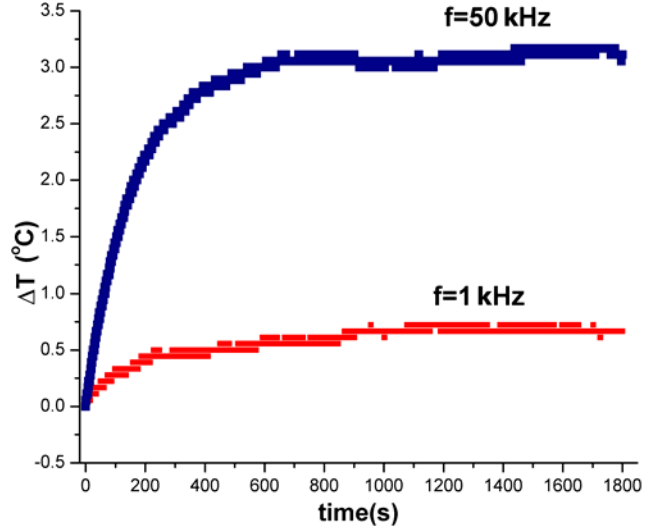


Fig.12. Temperature response of DFN cell exposed to air after the voltage  $U_{rms} = 20$  V were applied.

The stationary value of temperature raise  $\Delta T$  of the LC film fits the model very well. Figure 11 demonstrate an excellent agreement with  $\Delta T \propto U_{rms}^2$ . The frequency dependence  $\Delta T \propto f\epsilon''(f)$  under the constant amplitude of applied voltage, Fig.10, shows that the dispersion of dielectric permittivity of LC can be satisfactorily described by the standard Debye-type relaxation process with a Debye relaxation time  $\tau_D$  [9]:

$$\epsilon''(f) = \frac{(\epsilon^L - \epsilon^H)f\tau_D}{1 + f^2\tau_D^2} \quad (13)$$

where  $\epsilon^H$  and  $\epsilon^L$  are the asymptotic values of  $\epsilon$  above and below the characteristic frequency  $f_D = \tau_D^{-1}$ , respectively. All frequencies except the lowest one ( $f = 1$  kHz) are above the threshold frequency, thus Eq.(13) should be used for perpendicular component of dielectric permittivity tensor. The presented results show that the temperature change of DFN cell with outside thermal stabilization is less than  $3^\circ C$ .

The DFN cell exposed to air showed a wider range of the temperature change and a slower temperature response because of low heat conductivity of air,  $G \sim 0.02 W/m.^0C$  at room temperature [11], see Fig.12.

## 5. Conclusion

We demonstrated the scheme of fast liquid crystal display based on dual frequency nematic cells. We observed time delay, which accompanied the fast optical retardation switching in dual frequency nematic cell driven by square waveform applied voltage. We analyzed the dielectric heating phenomenon, and demonstrated that this effect can be controlled to maintain the operating temperature of the cell constant.

We thank Phil Bos, Ivan Smalyukh, and Yuriy Nastishin for helpful discussions.

1. Handbook of Optics (Devises, Measurements, &Properties) vol. II/sponsored by the Optical Society of America; Michael Bass, editor in chief, -2nd edition.
2. McManamon , P. F., Dorschner, T. A., Barnes, L. J., Optical Engin., 32, 2657 (1993); McManamon, P. F., Dorschner, T. A., Corkum, D. L., Friedman, L., Hobbs, D. S., Holz, M., Liberman, S., Nguyen, H. Q., Resler, D. P., Sharp, R. C., Watson, E. A., Proc. IEEE 84, 268 (1996).
3. Dayton, D., Browne, S., Gnglewski, J., Restaino, S., Appl. Opt., 40, 2345 (2001).
4. Blinov, L. M., Chigrinov, V. G., Electrooptic Effects in Liquid Crystal Materials, 133-234, Springer-Verlag: New York, (1994).
5. Wu, S. T., Neubert, M.E., Keast, S. S., Abdallah, D. G., Lee, S. N., Walsh, M. E., Dorschner, T. A., Appl. Phys. Lett., 77, 957 (2000).
6. Golovin, A. B., Shiyanskii S. V., Lavrentovich, O. D., Appl. Phys. Lett., 83, 3864 (2003); Golovin, A. B., Shiyanskii S. V., Lavrentovich, O. D., SID digest, 2, 1472, (2003).
7. Born, M., Wolf, E., Principle of Optics. 7th ed. Cambridge: Cambridge, UK, (1999).
8. Debye, P., Polar Molecules. Dover: New York, (1929).
9. Schadt, M., Mol. Cryst. Liq. Cryst., 319, 336 (1981).
10. Daudeville L., Carre H., J. of Thermal Stresses 21, 667 (1998).
11. Lide D. R., Handbook of Chemistry and Physics, CRC Press 83<sup>rd</sup> edition, Boca Raton, Florida USA, (2003)